Supporting Information

Boosting hydrogen evolution and triiodide reduction via electronic coupling on (1T, 2H) MoS_2@N-doped carbon dodecahedron

Lan Yu[1#], Chengxu Liu[1#], Li Sun[1], Wei Kan[1], Ying Xie[2], Xiuwen Wang[1]*, Yuying Cao[1], Bing Zhao[1]*, Chunmei Lv[1]*

[1] Heilongjiang Provincial Key Laboratory of Surface Active Agent and Auxiliary, College of Chemistry and Chemistry Engineering, Qiqihar University, Qiqihar, 161006, China.

Email: xwwang@qqhru.edu.cn; zhao_submit@aliyun.com; 03291@qqhru.edu.cn.

[2] Key Laboratory of Functional Inorganic Material Chemistry, Ministry of Education, Heilongjiang University, Harbin, 150080, China.

[#] These authors are contributed equally to this work.

1. Experimental details

1.1 Materials

All chemicals are used as received without any further purification. The sodium molybdate dihydrate ($Na_2MoO_4 \cdot 2H_2O$), 2-methylimidazole, acetonitrile, zinc acetate dihydrate ($Zn(CH_3COO)_2 \cdot 2H_2O$), glucose, thiourea, polyvinylidene fluoride, and potassium hydroxide (KOH) were purchased from the Aladdin Reagent Co., Ltd. The hydrochloric acid (HCl), ethanol, and acetone were obtained from the Tianjin Kemiou Chemical Reagent Co., Ltd. The redox shuttle electrolyte was a blend of 0.1 M LiI (anhydrous, 99%, Acros), 0.05 M I_2 (anhydrous, 99.8%), 0.5 M tert-butylpyridine (99%, Aldrich), 0.1 M guanidine thiocyanate (99%, Aladdin Co.) and 0.6 M 1-propyl-2, 3-dimethylimidazolium iodide (99%) in methoxyacetonitrile (99%, Fluka). The Nafion (5 wt%) was obtained from Sigma-Aldrich. The used Ru complex dye was *cis*-bis(isothiocyanato)bis(2,2'-bipyridyl-4,4'-dicarboxylato) ruthenium (II) bistetrabutyl-ammonium (N719, Solaronix SA, Switzerland). H_2PtCl_6 were purchased from the Sinopharm Chemical Reagent Co., Ltd. The conductive substrate is fluorine doped SnO_2 glass (FTO, 15 Ω/square, Nippon sheet glass, Japan).

1.2 Preparation of HER electrodes

The working electrode was prepared by mixing 5 mg of catalyst (MoS_2@NC, MoS_2, NC, Pt/C, MoS_2@NC-1, and MoS_2@NC-3) in the ethanol/deionized water (v/v=1:1, total volume is 1 mL). Then the 10 μL of Nafion (5 wt%) solution was added to the above mixture. The mixture was treated to obtain a dispersed slurry. The slurry was pasted on a piece of carbon cloth (1.0 cm × 1.5 cm), and then used as work electrode for HER in 1.0 M KOH.

1.3 Preparation of CEs and assembly of DSSCs

The FTO (1.5 cm×2.0 cm) was cleaned with acetone, ethanol, and deionized water, respectively. The MoS_2@NC (90 wt%) and polyvinylidene fluoride (10 wt%, binder) were mixed together with the certain amount of the N-methyl-2-pyrrolidone, followed by stirring and sonication to form the viscous slurry. Then the uniform catalyst films were covered on the surface of a cleansed FTO glass by doctor-blade technique, and sintered in a tube furnace for 1 h at 400 °C under N_2 atmosphere. The coating amount of CE catalysts can be controlled by pre-pasting special tape on the FTO conductive substrate. For comparison, the pyrolytic Pt CE was prepared by drop-casting H_2PtCl_6 (50 μL) in ethanol (5 mM) on the cleansed FTO glass and raised reaction temperature to 385 °C for 30 min under air atmosphere.

The dye-sensitized TiO_2 photoanodes were prepared by the standard method. DSSCs assembled into a sandwich structure with the N719 loaded TiO_2 photoanode, iodine-based electrolyte containing redox couple (I_3^-/I^-), and CEs (Pt and MoS_2@NC). The redox shuttle electrolyte was injected into the space between the photoanode and CE. In order to prevent the electrolyte solution leakage, two electrodes were adhered together with thermoplastic hot-melted surlyn. Moreover, the fabrication of symmetric cells is similar to that of the above DSSCs, except that the two same CEs are used and assembled them together with surlyn.

1.4 Characterizations and measurements

Raman spectroscopy was measured by the Invia spectrometer with an excitation laser wavelength of 532 nm. X-ray photoelectron spectroscopy (XPS) was carried out by using a model of VG ESCALAB MK II with an Mg Ka (1253.6eV) achromatic X-ray source. Scanning electron microscopy (SEM) was carried out by the Hitachi S-4800 microscope. Transmission electron microscopy (TEM), high-resolution TEM (HRTEM), and EDX mapping images were obtained from JEM-3010 (JEOL) with a voltage of 200 kV. The electrochemical measures were conducted on a CHI760E electrochemical workstation (Shanghai Chenhua Instrument Corp., Shanghai, China).

For HER performance test: The as-prepared samples were uses as work electrode, as mentioned above. The standard Hg/HgO and graphite rod was employed as the reference electrode and counter electrode during HER performance tests in alkaline medium, respectively. The linear sweep voltammogram (LSV) was conducted at a 5 mV/s scan rate after 20 cycles of CV tests to stabilize the current. To exclude the effect of resistance from solution and electrode, an 80 % iR compensation was employed in the electrochemical measurement of LSV. The Nyquist plots can be obtained at the frequency range of 0.01-100,000 Hz. The electrochemical doublelayer capacitance (C_{dl}) of catalysts can be calculated by fitting CV curves at different scan rates in non-Faradaic potential range. The turnover frequency (TOF) can be estimated according to this equation: TOF = $I/2nF$, where I represent the current density for different samples, F is the Faraday constant (C/mol), n is the number of the active sites (mol) for samples. Long-term stability was evaluated by performing 1000 cycles of CV at a scan rate of 5 mV s^{-1} over selected potential ranges, chronoamperometric curves were conducted for 48 h.

J-V curves of DSSCs were measured under a solar simulator (AM 1.5). Cyclic voltammetry (CV) was carried out in the typical three-electrode system. Specifically, the MoS_2@NC and Pt CEs worked as a working electrode, Ag/AgCl was used as a reference electrode, and the commercial Pt plate was used as a counter electrode. The supporting electrolyte for CV curve was an anhydrous acetonitrile solution of 0.1 M $LiClO_4$, 10 mM LiI, and 1mM I_2, and the potential range was from -0.6 V to 1.2 V. Electrochemical impedance spectroscopy (EIS, bias voltage: 0 mV; frequency range: 0.01 Hz to 100 kHz; disturbance voltage: 10 mV) and Tafel polarization data were assembled as the style of the symmetrical cells which were full of the identical electrolyte. The obtained EIS data were fitted by the Z-View software in terms of appropriate equivalent circuits.

1.5 DFT calculation details

All theoretical calculations based on DFT were carried out using the Vienna ab initio simulation package (VASP)[1]. Perdew-Burke-Ernzerhof functional with a generalized gradient approximation (GGA-PBE) form was adopted to deal with the exchange correlation energies of the systems[2]. The plane-wave and pseudo-potential techniques were used, and the energy cutoff was 400 eV. To obtain a good numerical sampling of electron densities in Brillouin zone, a (2×2×1) Monkhorst-Pack mesh was applied to the MoS_2 (002) and MoS_2@NC surface. The optimization procedure was repeated until the maximum residual force is less than 0.05 $eV\cdot Å^{-1}$ in any directions. During the calculations, a vacuum layer of 15 Å is used to avoid the fake interactions between periodic images along z axis. Visualization of the atomic structures are made by using VESTA[3]. The MoS_2@NC and MoS_2 was simulated to investigate alkaline

HER mechanism. The adsorption Gibbs free energy of reaction intermediates (ΔG) is defined as:

$$\Delta G = \Delta E + \Delta E_{ZPE} - T\Delta S$$

where ΔE is the DFT energy difference of each step, ΔE_{ZPE} is the correction of zero point energy, ΔS is the variation of entropy obtained by vibration analysis, T is the temperature (T = 298.15 K).

References

1. G. Kresse and J. Furthmüller, Efficient iterative schemes for ab initio total-energy calculations using a plane-wave basis set, *Phys. Rev. B*, 1996, **54**, 11169-11186.
2. B. Hammer, L. B. Hansen and J. K. Nørskov, Improved adsorption energetics within density-functional theory using revised Perdew-Burke-Ernzerhof functionals, *Phys. Rev. B*, 1999, **59**, 7413-7421.
3. K. Momma and F. Izumi, VESTA 3 for three-dimensional visualization of crystal, volumetric and morphology data, *J. Appl. Crystall.*, 2011, **44**, 1272-1276.

2. Supporting data

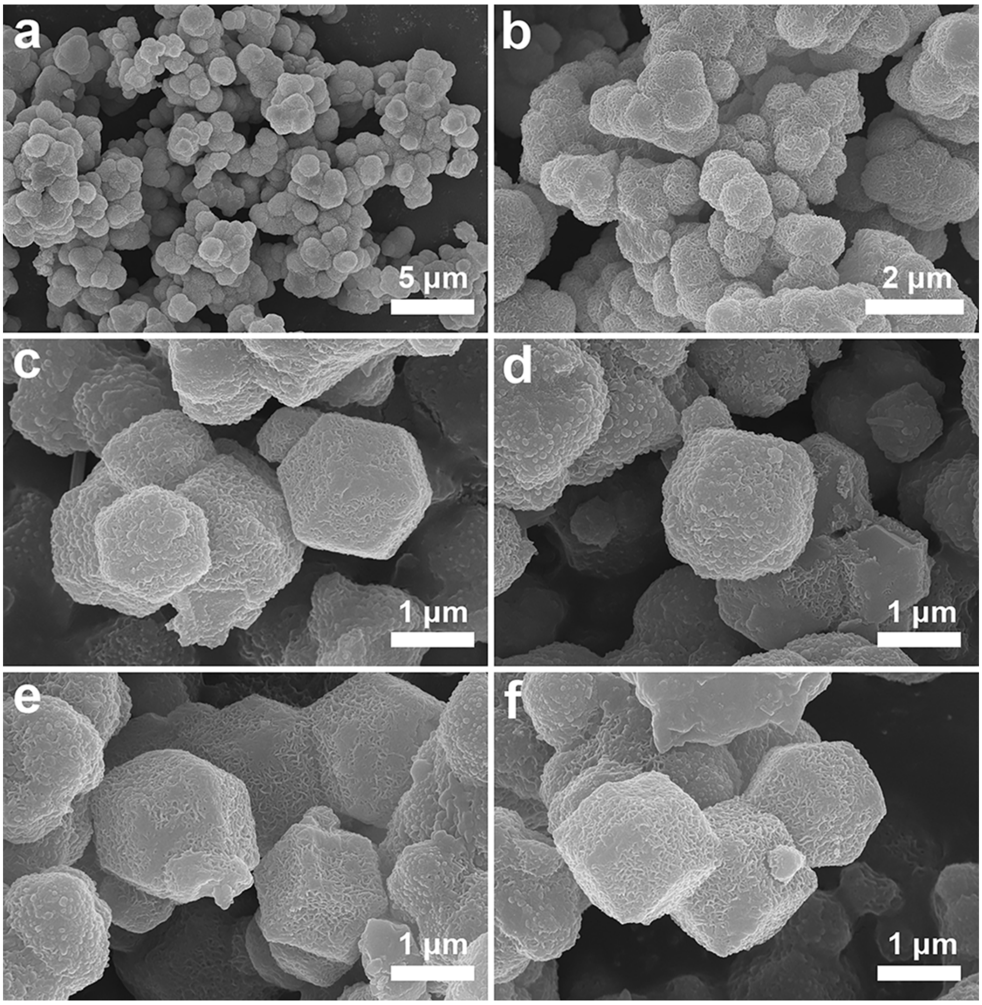

Fig. S1 SEM images of (a, b) MoS_2, (c, d) MoS_2@NC-1, and (e, f) MoS_2@NC-3.

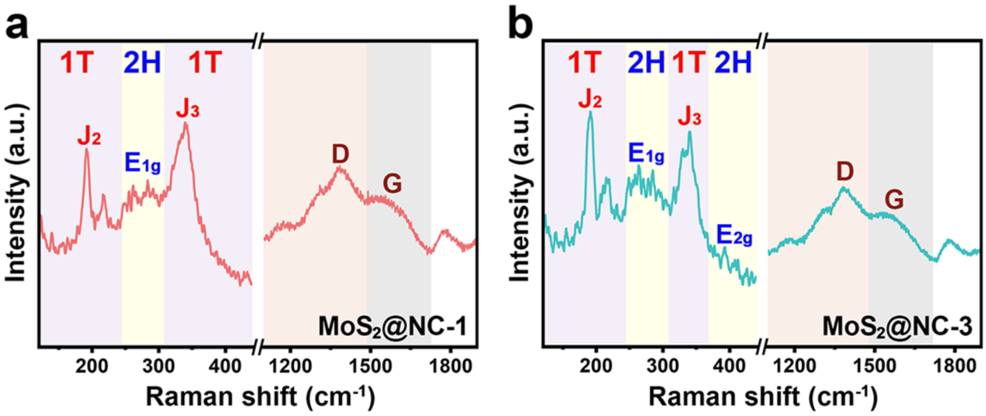

Fig. S2 Raman spectra of (a) MoS_2@NC-1 and (b) MoS_2@NC-3.

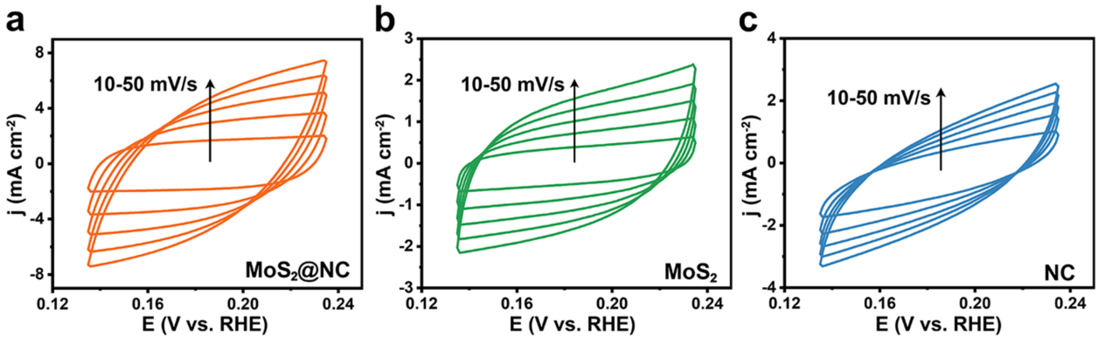

Fig. S3 CV curves measured in a non-Faradaic range at different scan rates (from 10 to 50 mV s^{-1}) of obtained catalysts: (a) MoS$_2$@NC, (b) MoS$_2$ and (c) NC.

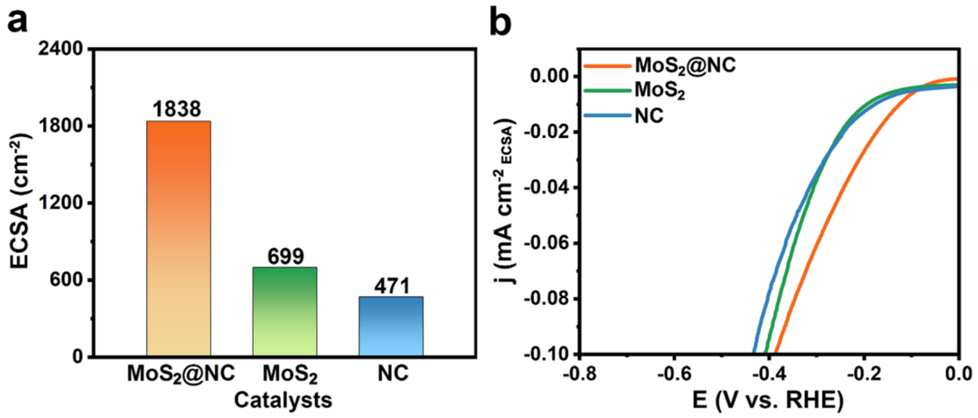

Fig. S4 (a) ECSA value and (b) ECSA-normalized LSV curves of MoS_2@NC, MoS_2, and NC.

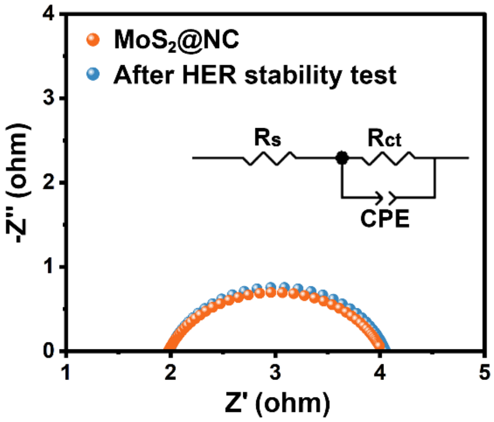

Fig. S5 Nyquist plots of MoS_2@NC before and after HER stability test.

Table S1 Comparison of HER performance of MoS_2@NC with recently reported MoS_2-based catalysts in 1.0 M KOH.

Catalysts	$\boldsymbol{\eta_{10}}$ **(mV)**	**References**
NiFe-LDH/MoS_2/CFP	88.5	Electrochim. Acta 2023, 467, 143079.
CN/CNL/MoS_2/CP	106	Chem. Eng. J. 2021, 412, 128556.
Co-1T-MoS_2-bpe-350	118	Angew. Chem. Int. Ed. 2023, 62, e202313845.
MoS_2@Cu	130	Mater. Chem. Phys. 2024, 318, 129234.
MoS_2/MoN	132	J. Alloys Compd. 2021, 867, 159066.
Co-NiS/Mo_2S_3	142	Int. J. Hydrogen Energy 2024, 62, 532-540.
FD-MoS_2-5	164	Nat. Commun. 2022, 13, 2193.
vr-1T MoS_2	184	Appl. Catal. B 2024, 352, 124037.
MoS_2/$NiFe_2O_4$	190	Int. J. Hydrogen Energy 2024, 69, 261-271.
LrGO-ZnO/1T-2H MoS_2	191.5	Mater. Today Energy 2024, 45, 101683.
HEO-MoS_2	214	South African J. Chem. Eng. 2024, 48, 425-435.
LSC/MoS_2	284	J. Mater. Chem. A 2024, 12, 8757-8768.
Ni-MoS_2	302	Int. J. Hydrogen Energy 2022, 47, 37256-37263.
0.2rGO-MoS_2	314	Chem. Eng. J. 2021, 418, 129343.
MoS_2@NC	**93**	**Our work**

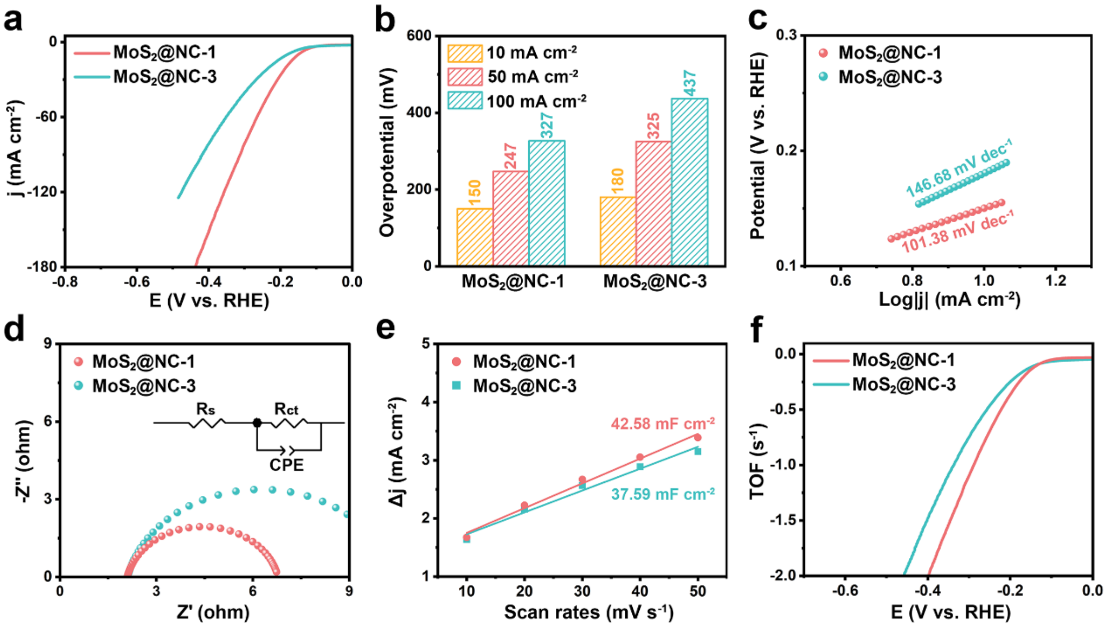

Fig. S6 HER performance of MoS_2@NC-1 and MoS_2@NC-3: (a) LSV curves, (b) Comparison of the overpotential at various current densities, (c) Tafel plots, (d) Nyquist plots, (e) C_{dl}, and (f) TOF.

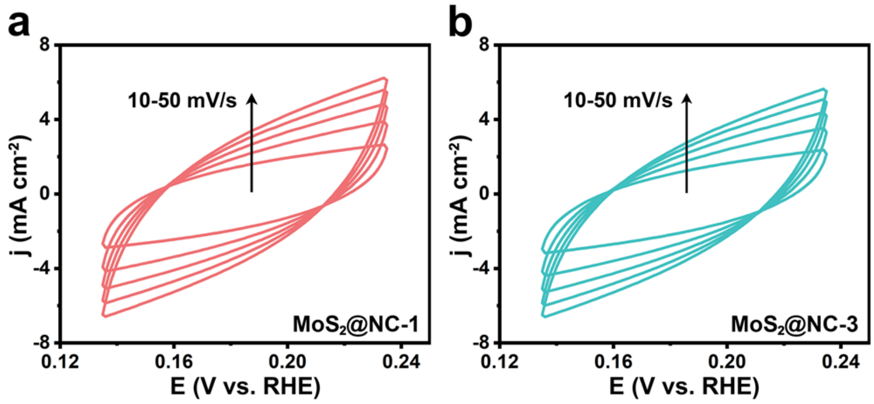

Fig. S7 CV curves measured in a non-Faradaic range at different scan rates (from 10 to 50 mV s^{-1}) of (a) MoS$_2$@NC-1 and (b) MoS$_2$@NC-3.

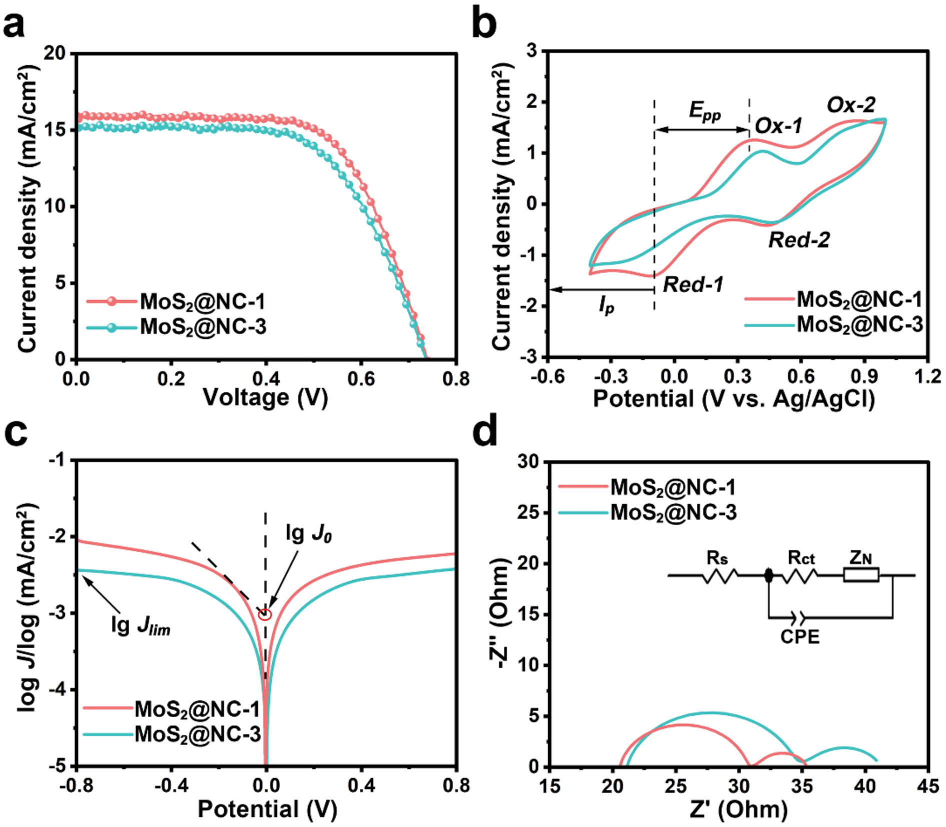

Fig. S8 (a) J-V curves, (b) CV curves, (c) Tafel polarization curves, and (d) Nyquist plots based on MoS_2@NC-1 and MoS_2@NC-3 CEs.

Table S2 Photovoltaic performance parameters of DSSCs based on various CEs.

CEs	**V_{oc} (V)**	**J_{sc} (mA/cm^2)**	***FF***	***PCE* (%)**
Pt	0.744±0.004	17.09±0.12	0.68±0.01	8.59±0.09
MoS_2@NC-1	0.739±0.005	15.98±0.13	0.65±0.02	7.72±0.14
MoS_2@NC	0.739±0.003	16.54±0.11	0.67±0.03	8.20±0.12
MoS_2@NC-3	0.736±0.002	15.10±0.11	0.64±0.01	7.07±0.10

Table S3 Comparison of *PCE* with recently reported MoS_2-based CE catalysts.

CEs	***PCE* (%)**	**References**
MNCS-2	6.20	RSC Adv. 2017, 7, 13433-13437.
MoS_2/rGO	6.72	Mater. Res. Bull. 2019, 117, 78-83.
MoS_2@RGO	6.82	J. Alloys Compd. 2018, 731, 685-692.
MoS_2@carbon	6.93	Sol. Energy 2017, 157, 948-955.
MoS_2/G	7.18	Nanoscale 2015, 7, 10459-10464.
CuS/MoS_2	7.21	Sol. Energy 2018, 171, 122-129.
CoS/MoS_2	7.48	J. Alloys Compd. 2018, 739, 568-576.
MoS_2/graphene	7.86	J. Power Sources 2017, 351, 58-66.
MoS_2/graphene	8.01	RSC Adv. 2016, 6, 34546-34552.
MoS_2 microspheres	8.45	Nanomaterials 2020, 10, 1725.
FeS_2/MoS_2	8.67	Sci. China Mater. 2018, 61, 1278-1284.
MoS_2@NC	**8.20**	**Our work**

Table S4 Electrochemical parameters of various CE catalysts.

CEs	E_{pp} (V)	I_p (mA/cm^2)	R_s (Ω)	R_{ct} (Ω)	J_0 (mA/cm^2)	J_{lim} (mA/cm^2)
Pt	0.43	-2.09	17.78	7.87	-2.71	-1.80
MoS_2@NC-1	0.50	-1.41	20.49	10.14	-3.02	-2.02
MoS_2@NC	0.49	-1.77	20.02	8.99	-2.76	-1.90
MoS_2@NC-3	0.67	-1.14	21.07	13.20	-3.34	-2.44

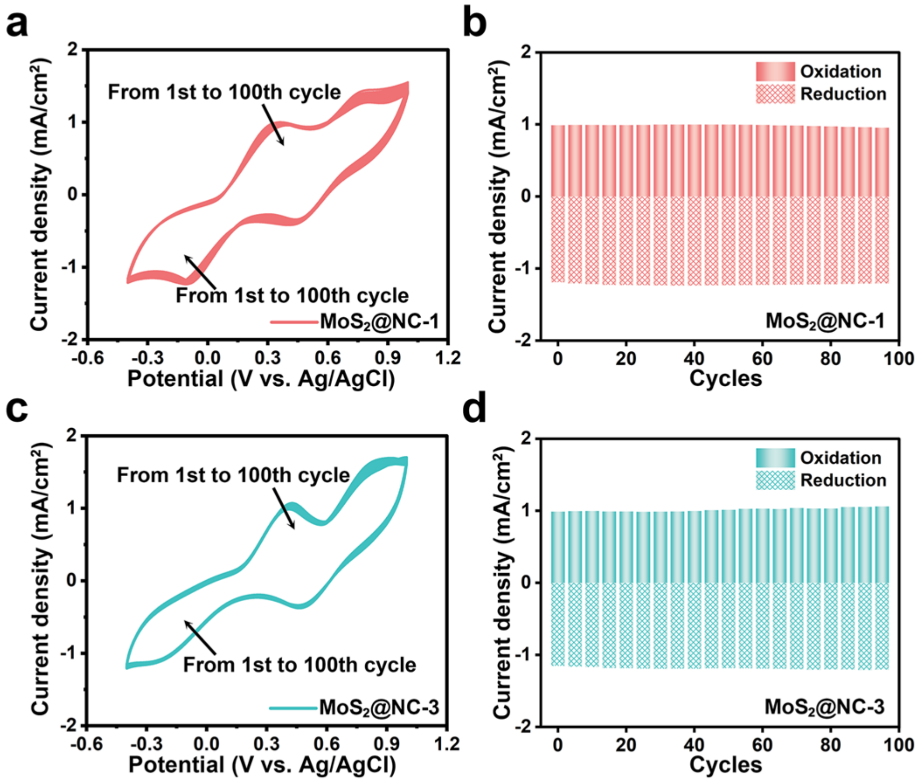

Fig. S9 100 consecutive CV curves and the corresponding anodic and cathodic peak current density vs. cycles for (a, b) MoS_2@NC-1 and (c, d) MoS_2@NC-3.

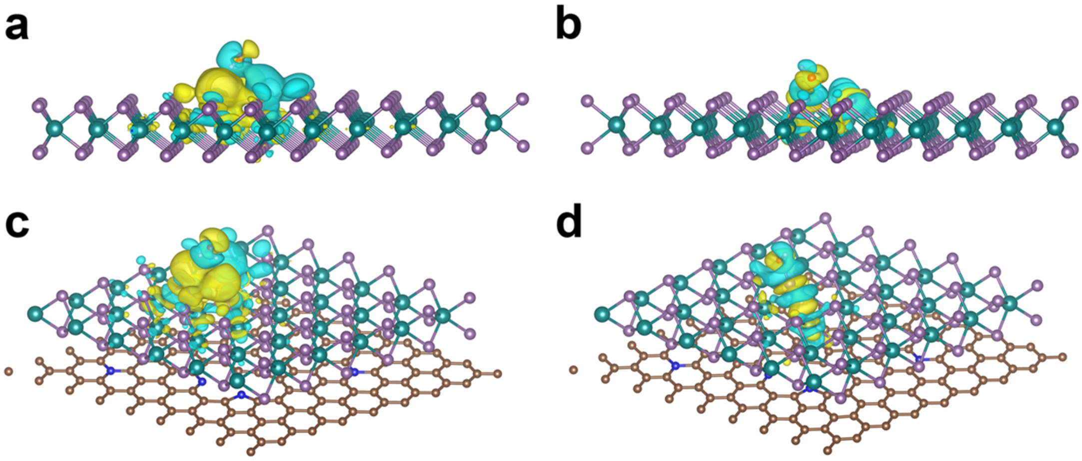

Fig. S10 CDD of (a, b) MoS_2 and (c, d) MoS_2@NC during RDS processes.